Hindawi
International Journal of Aerospace Engineering
Volume 2018, Article ID 1594570, 14 pages
https://doi.org/10.1155/2018/1594570

Research Article

The Aerodynamic Behavioral Study of Tandem Fan Wing Configuration

Du Siliang[1] **and Tang Zhengfei**[2]

[1]*Faculty of Mechanical & Material Engineering, Huaiyin Institute of Technology, Huaian 223003, China*
[2]*National Key Laboratory of Rotorcraft Aeromechanics, Nanjing University of Aeronautics and Astronautics, Nanjing 210016, China*

Correspondence should be addressed to Du Siliang; kjofchina@qq.com

Received 5 February 2018; Accepted 16 August 2018; Published 30 October 2018

Academic Editor: Kenneth M. Sobel

The fan wing aircraft is a new concept based on a new principle, especially its wing which is based on a unique aerodynamic principle. A fan wing can simultaneously generate lift and thrust. In order to further improve its aerodynamic characteristics without changing its basic geometric parameters, two fan wings are installed along the longitudinal body, which is the composition of a tandem fan wing aircraft. Through numerical simulation, the lift and thrust of the fan wings were calculated with the distance, height, and installation angle of the front and rear fan wings changed, and the aerodynamic characteristic interaction rule between the front and rear fan wings was analyzed. In addition, the wind test model of a tandem fan wing was designed, and the results of the wind tunnel test and numerical calculation results were compared to verify the preliminary setup. The results show that at a certain height, distance, and installation angle, aerodynamic characteristics of a tandem fan wing have more advantages compared to the single fan wing. Therefore, the tandem fan wing aircraft's advantages have good prospects for development and application.

1. Introduction

A fan wing aircraft [1–4] has a crossflow fan at the leading edge of each wing. The fan, powered by a conventional engine, pulls the air in from the front and accelerates the air over the trailing edge of the wing. By transferring the power of the engine to the crossflow fan, which spans the whole wing, the fan wing accelerates a large volume of air and produces lift and thrust simultaneously. It cannot be classified as either a fixed wing or rotary aircraft but shares certain fundamental features of both. The fan wing concept with distributed propulsion is described as a simple, stable, and very efficient high lift aircraft. The implementation of a crossflow fan in a wing was first proposed by Nikolaus Laing in 1964 [5], who together with Bruno Eck are responsible for increasing the crossflow fan efficiency. Hancock [6] worked on raising the efficiency of the crossflow fan implementation at Lockheed up to the value of 82%. However, the fan was reported to be so noisy that the test area had to be evacuated during the tests and was never integrated into a wing. The subsequent research studied the flow field through the crossflow fan with high- and low-pressure cavities [7]. Recently, the investigations on the fan wing technology integrated in airfoils showed the high lift potential of the embedded propulsion system and moved the research from experimentation to prototyping [8]. It exhibits great potential for exploitation in a wider range of commercial or military applications.

The implementation of a single fan wing was numerically and experimentally investigated [9–15]. The results confirmed the high lift, fuel consumption reduction, and noise decreasing characteristic. However, the studies above are all conducted on a single fan wing; with reference to the tandem wing aircraft [16] and tandem rotor helicopter [17], we proposed the tandem fan wing aircraft (two fan wings installed along the longitudinal body). This kind of aircraft realizes the flight capability to take off and land at ultrashort distances or vertically with the heavy load, which satisfies the demand for an aircraft at low speed with a heavy load in some particular situations. This paper is aimed at studying

a tandem fan wing configuration by CFD method, including the force measurement experiments in the wind tunnel.

2. Model and Calculation Method

2.1. Tandem Fan Wing Model. The layout of the tandem fan wing is shown in Figure 1. We defined the geometric parameters of the single fan wing model (Figure 2, Table 1) and blade geometric parameters (Figure 2(b), Table 2). The geometric parameters of the front and rear wings are the same.

2.2. Calculation Method. In this paper, the maximum rotation speed of the crossflow is 2000 r/min, and the blade tip's rotation speed of the crossflow fan is less than 0.3 Ma. Therefore, the compressibility of airflow can be ignored in the numerical calculation. The whole flow field around the fan wings is in an unsteady state, and it is necessary to take the influence of the Reynolds number into account [18]. The numerical simulations are performed using the commercial general-purpose CFD code FLUENT 14.5 by Fluent Inc. The ANSYS ICEM software was used for grid division. For the CFD analysis, free stream velocity and angle of attack are constant for all rotation velocities. Renormalization group (RNG) $k-\varepsilon$ model was used for turbulence. The pressure-velocity coupling was calculated using the SIMPLEC algorithm. Second-order upwind discretization was considered for the convection terms. The finite volume method with rectangular elements was used for the whole solution domain. The rotating and stationary domains connected each other with a fluid-fluid interface, where the flow continuity is satisfied. To simulate the fan rotating, the area surrounding the blades was designed as a sliding mesh region (Figure 3). A uniform velocity is imposed at the inlet, while a zero relative static pressure is prescribed at the outlet. Unsteady simulations require a proper setting of both the time step size and the convergence criteria within each time step. For this simulation, a time step size equal to 1/20th of the blade passing period captured the unsteady flow well. Within each time step, iterations were performed until the solution no longer changed. It was found necessary to reduce all residuals to at least 10^{-5}. With these, we set up the numerical calculation model for analysis of different distances, heights, and installation angles between the front and the rear wing.

2.3. Example Verification. We took the wind tunnel test results from the literature [19] to verify the accuracy of the numerical simulation method. Given the coming flow, speed of 10 m/s, angle of attack of 0°, and range of crossflow fan rotation speed changing within 400–1200 r/min, we made a contrastive verification of the lift and the thrust of the single fan wing. Figures 4(a) and 4(b) show the test results of the lift and the thrust of the single fan wing at the different rotation speeds of the crossflow fan. As we can see from the pictures, with the increase of crossflow fan rotation speed, the lift and the thrust gradually increased as well, and the calculation results coincide with the trend of test results well with the maximum error less than 10%. Therefore, the numerical method mentioned above can be used in the calculation and analysis of the tandem fan wing aerodynamic characteristics. It can be seen from the curve that when the speed is 1000 r/min, the lift and thrust errors have a minimum value of 0.17 N and 1.04 N, respectively. We use the rotational speed at this time as the reference speed for calculation and analysis.

3. Calculation Results and Analysis

3.1. The Relationship between the Aerodynamic Force and the Distance. Figure 5 shows the definition of the tandem fan wing model with different distances. The height and the angle between the front and the rear wings are zero; we calculated the aerodynamic force with different distances of 500 mm, 600 mm, 700 mm, 800 mm, 900 mm, and 1000 mm (such six conditions).

Figures 6(a) and 6(b) show, respectively, the changing curve of the lift and the thrust's variation following the distance between the front and the rear wings. As you can see from Figure 6(a), the lift force increases with distance when under 700 mm. On the contrary, when over 700 mm, the lift tends to be stable when the distance changes. In addition, the front wing's lift is always greater than the rear wing's, and compared with the single fan wing, the increase of the rear wing's lift is relatively small, even less than the single fan wing's lift when the distance decreases to some extent. On the whole, the average aerolift effect of the tandem fan wing is better than that of a single fan. According to the figures, it has increased by about 27%. After analysis of the force curve in Figure 6(b), we can find that tandem fan wings' added value of thrust is quite smaller than the single wing's when the distance is big. Only when the distance is minimum does the tandem fan wing have its advantage, increasing the thrust by about 51%.

In order to further illustrate the principle of the aerodynamic increase of the tandem fan wing, we drew the velocity contours and streamlines with different distances between the front and the rear wings in Figure 7. As we can see from these figures, due to the interactive influence of the front and the rear airflow, the intensity and position of the low-pressure vortices inside the fan wing are different. With reference to the single flow chart of the flow velocity, when spacing is small, most of the airflow accelerated by the front wing flows into the rear wing, which will be accelerated again by the crossflow fan in the rear fan wing. Therefore, the airflow speed of the rear fan wing is always larger than the front one. When the distance is over or equal to 700 mm, the rear wing's acceleration of airflow from the front wing decreases, most of which escape the rear fan wing's acceleration, which means the flow into the rear wing decreases. Therefore, the rear fan wing's lift is always less than the front fan wing's.

Now we talk about the front and the rear wings' impact on the change of thrust. The thrust produced by the fan wing derives from the acceleration of airflow by the crossflow fan's rotation. When the spacing is small, all the airflow out of the front wing flows into the rear wing, and the flow rate of accelerated flow in the crossflow fan increases in unit time. According to Newton's third law, the crossflow fan's blade gets more reaction so that the rear wing's thrust gets larger

(a) Tandem fan wing layout

(b) Tandem fan wing UAV

Figure 1: Tandem fan wing.

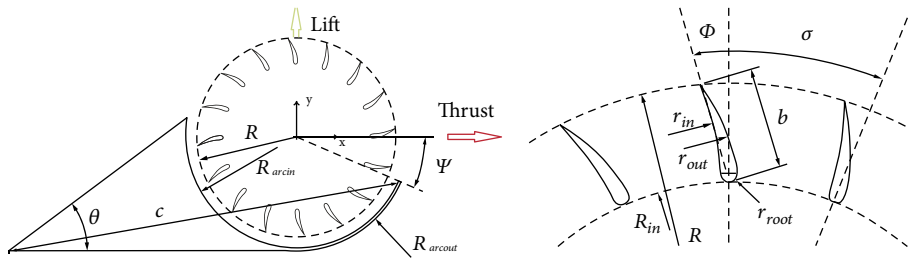

(a) Fan wing section geometry definition

(b) Crossflow fan blade geometry definition

Figure 2: Fan wing section.

Table 1: Definition of fan wing geometric parameters.

Definition	Value
Fan wing span L (mm)	500
Radius of crossflow fan R (mm)	150
Inner radius of semicircular cavity R_{arcin} (mm)	155
Outer radius of semicircular cavity R_{arcout} (mm)	160
Fan wing chord c (mm)	561
Trailing edge angle θ (°)	36.5°
Opening angle of the leading edge ψ (°)	24°

Table 2: Crossflow fan blade geometric parameters.

Parameters	Value
Blade width b (mm)	36
Outer radius of crossflow fan R (mm)	150
Inner radius of crossflow fan R_{in} (mm)	98
Blade outer arc radius r_{out} (mm)	96
Blade inner arc radius r_{in} (mm)	68
Blade root arc radius r_{root} (mm)	3
Blade installation angle ϕ (°)	18
Contiguous blade angle σ (°)	22.5

when the distance narrows. When the distance increases to 700 mm, the thrust of the front wing is the minimum and gradually increases at the same pace of distance. It may be caused by the flow velocity of the edge inclined plane effected by the rear fan wing.

3.2. The Relationship between the Aerodynamic Force and the Height. The definition of the tandem fan wing with different heights is shown in Figure 8. We defined the distance as 800 mm, and the angle between the front and the rear wings does not change. The height difference is $h/2R = 1, 2, 0, 0.5, 0.5$ (five conditions).

Figures 9(a) and 9(b) show the curves of the lift and the thrust of the front and the rear fan wings with different heights. It can be found that when the front fan wing is relatively higher than the rear one, the effect on the lift of the front fan wing is significant, but the rear fan wing is not significant. When $h/2R = 0$, the lift increases to the maximum. The changes of the height difference between the front and the rear wings have little influence on the overall thrust, and the relationship between the thrust of the front and the rear wing shows the opposite trend. Figure 10 shows the velocity contours and streamlines of the height change between the front and rear wings of the tandem fan wing. As we can see, when $h/2R > 0$, airflow accelerated by the front fan wing from its trailing edge slope to the rotating crossflow fan of the rear fan wing is quite stable. When $h/2R = 0.5$, the lift of the front wing is small, which is caused by the

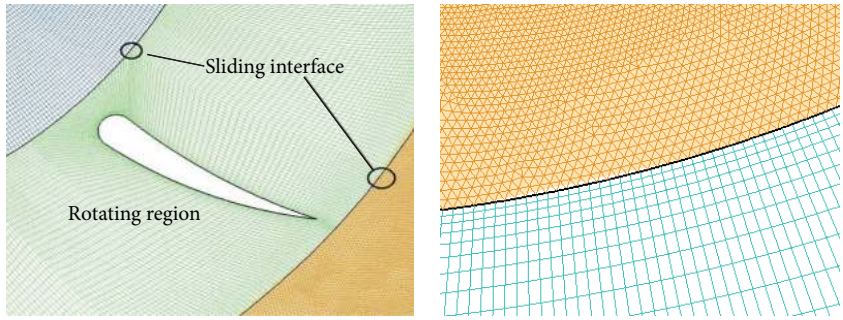

(a) Sliding mesh region (b) Grid details

Figure 3: Interface and grid definition.

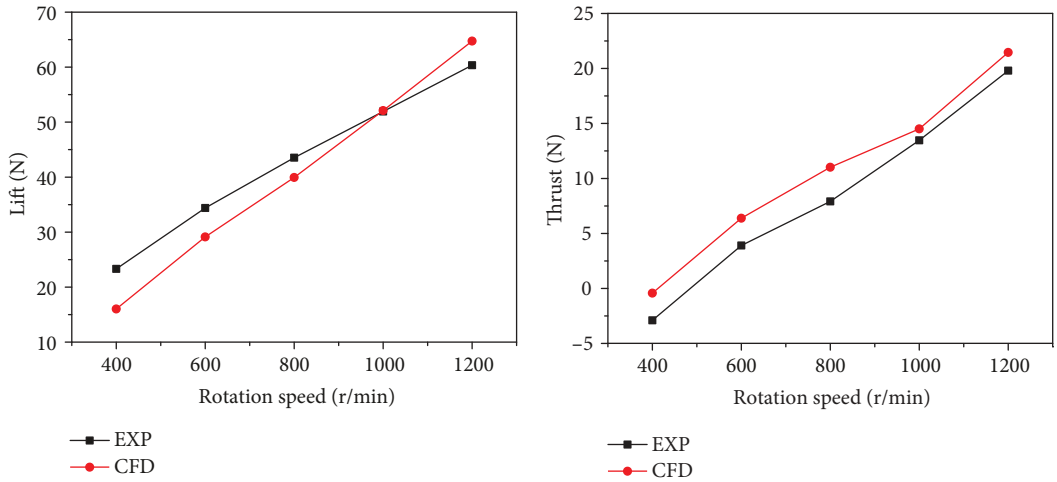

(a) Comparison verification of lift force (b) Comparison verification of thrust force

Figure 4: The numerical calculation results and test results with the crossflow fan speed change curve.

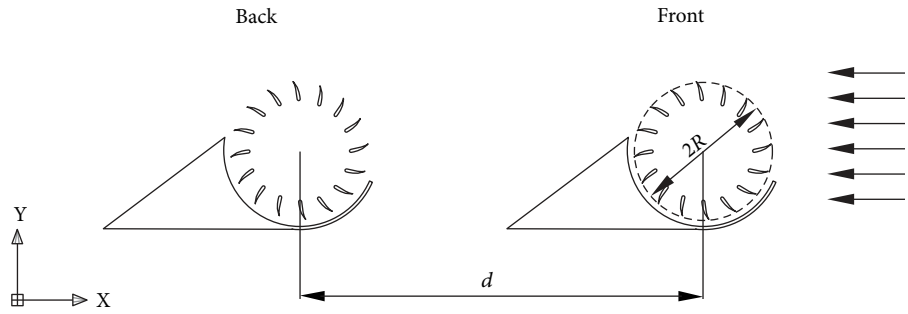

Figure 5: Definition of distance between front and rear wings of the tandem fan wing.

decreased pressure on the front wing's surface with the airflow acceleration from the rear wing. The $h/2R = 0.5$ value results in rather "odd" changes in lift and thrust behavior. This is due to the high energy fluid leaving the front fan wing entering the rear fan wing.

3.3. The Relationship between the Aerodynamic Force and the Installation Angle. Figure 11 shows the definition of the tandem fan wing with different installation angles between the front and rear wings. We defined the distance as 800 mm, the height difference between the front and the rear wings as $h/2R = 0$, and the installation angle of the front wing as 0°. Then we calculated the aerodynamic force when the installation angle of the rear fan wing is −20°, −10°, 0°, 10°, and 20°. Next, we defined the installation angle of the rear wing as 0° and calculated the aerodynamic force when

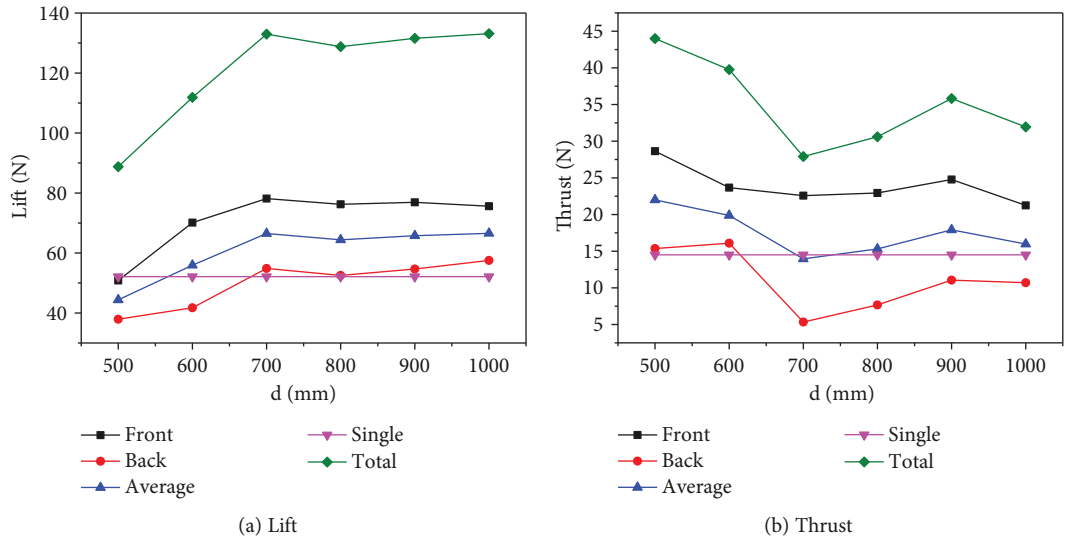

(a) Lift (b) Thrust

Figure 6: Tandem fan wing aerodynamic force with the changing curve following the distance between the front and rear wings.

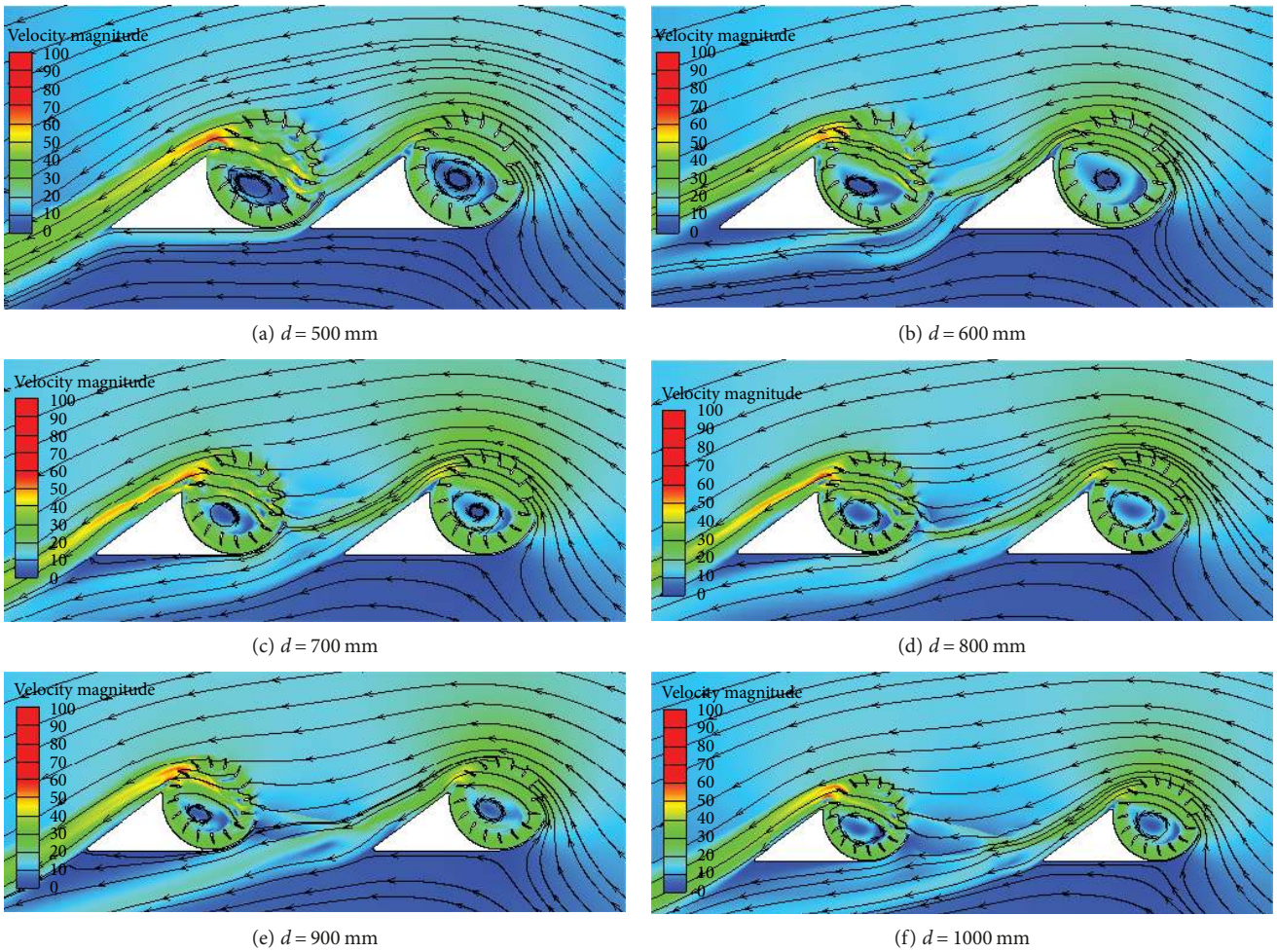

(a) $d = 500$ mm (b) $d = 600$ mm

(c) $d = 700$ mm (d) $d = 800$ mm

(e) $d = 900$ mm (f) $d = 1000$ mm

Figure 7: Velocity contours and streamlines of the distance change between the front and rear wings of the tandem fan wing.

the installation of the front wing is −20°, −10°, 0°, 10°, and 20°. Later, we calculated the aerodynamic force when the installation angles of the front and the rear wings are the same. Finally, we calculated the aerodynamic force when the installation angle of the front wing is negative to that of the rear wing.

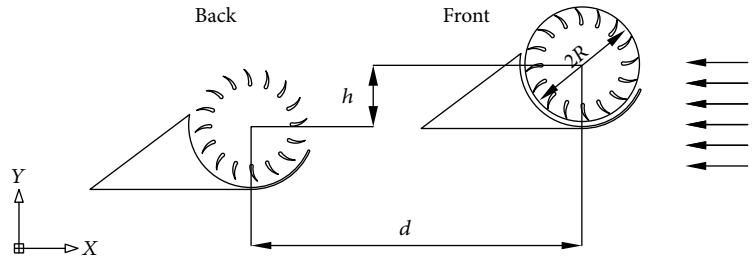

Figure 8: Definition of height between the front and rear wings of the tandem fan wing.

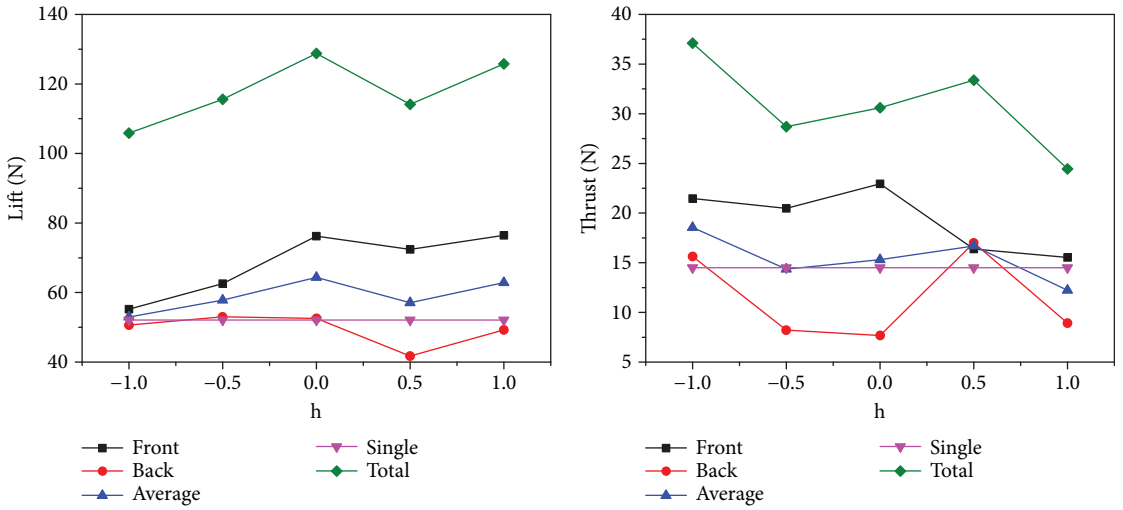

(a) Lift (b) Thrust

Figure 9: Tandem fan wing aerodynamic force with the changing curve following different heights between the front and rear wings.

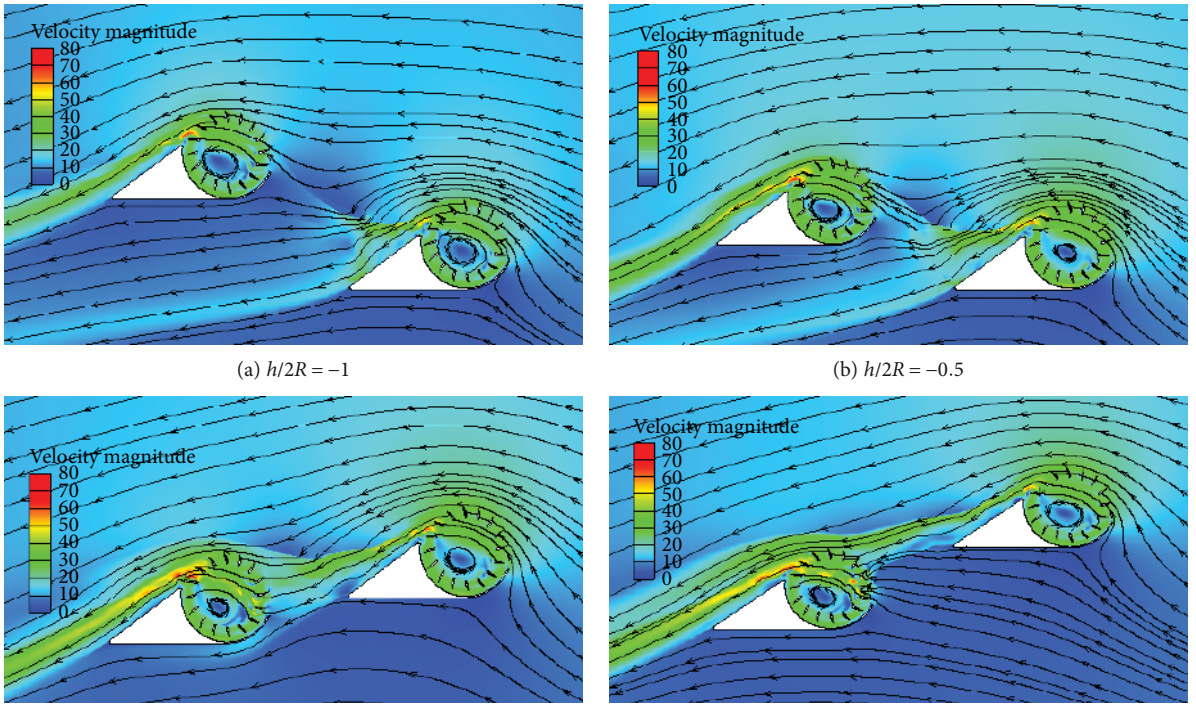

(a) $h/2R = -1$ (b) $h/2R = -0.5$

(c) $h/2R = 0.5$ (d) $h/2R = 1$

Figure 10: Velocity contours and streamlines of the height change between the front and rear wings of the tandem fan wing.

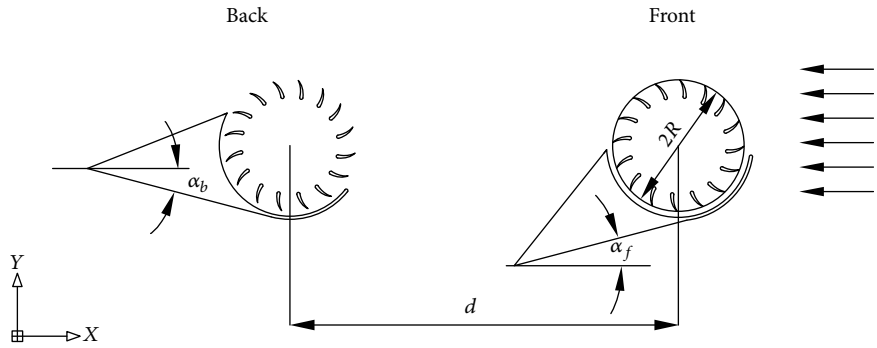

Figure 11: Definition of the angle between the front and rear wings of the tandem fan wing.

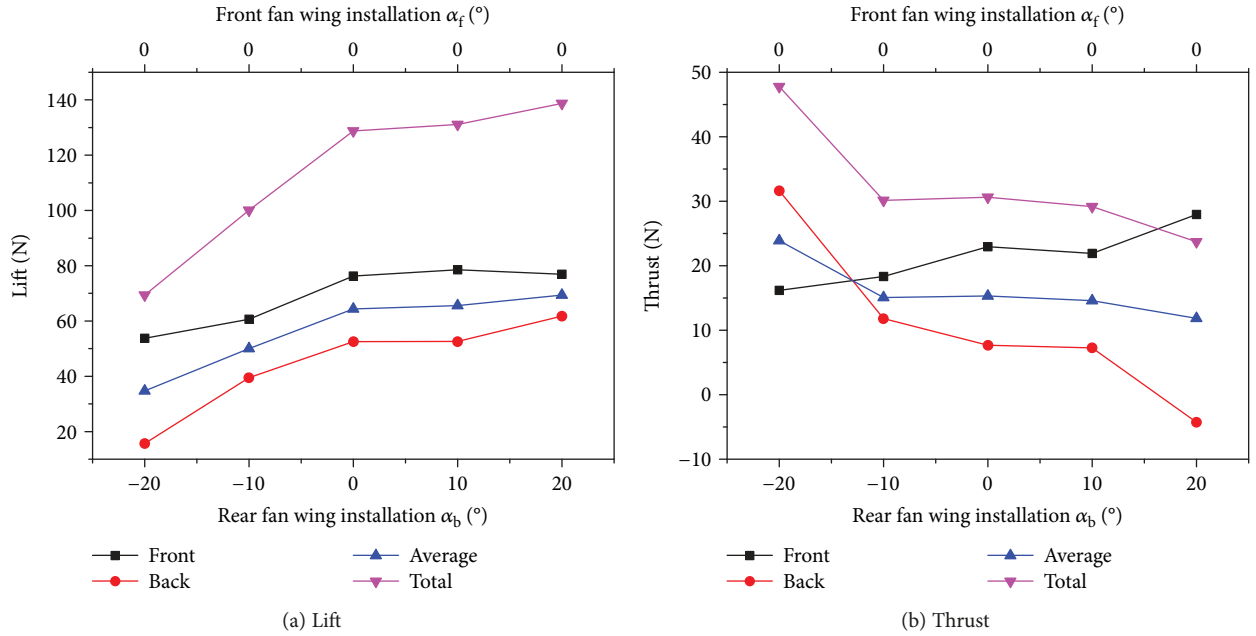

(a) Lift (b) Thrust

Figure 12: Curve of the lift and thrust of the front and rear fan wings when the front wing is fixed.

3.3.1. The Installation Angle of the Front Fan Wing Is Unchanged. As we can see from Figure 12(a), as the installation angle of the rear wing increases, the lift of both the front and the rear wings keeps pace with it, while the lift of the rear wing has a relatively great effect on that of the front wing, and it is about 20% more than the front wing's (the installation angle of the rear wing is 20°). However, when the installation angle of the rear wing is greater than or equal to 0°, the added value of the rear wing's lift hardly changes. From the average value of the front and the rear wing's lift, we can see that it is increasing all the time, and the overall aerodynamic increase is good. As we can see from Figure 12(b), the rangeability of the average thrust is not very large, and the thrust of the front and the rear wings shows the opposite trend. As is shown in Figure 13, when the installation angle of the rear wing is negative, the airflow of the front wing's trailing edge slope flows in an S-shaped path when across the rear wing's lower surface. When the installation angle of the rear wing is positive, basically, it flows along the airflow of the trailing edge slope, which illustrates that the rear wing has a good rectification effect on the front wing under this condition. The result at the rear angle > 0° is that the lift does not change much as most of the high energy fluid leaving the front fan wing does not enter the rear fan wing.

3.3.2. The Installation Angle of the Rear Fan Wing Is Unchanged. As we can see from Figure 14, when the installation angle of the front wing is greater than 0°, the lift of both the front and the rear wings tends to be stable. When the installation angle of the front wing ranges from −20° to −10°, lift of the rear wing is less than that of the front wing. With analysis of Figure 15, we can find that the accelerated airflow from the front wing just flows into the rear wing, due to the suction effect of the rear wing on the front wing's airflow, which increases the flow rate on the trailing edge wing surface of the front wing and decreases the relative pressure; all these contribute to the increase of the front wing's lift. From the average value of the front and the rear wings' lift, we can find that the average lift hardly changes, and the changes of the front wing's installation angle are insignificant

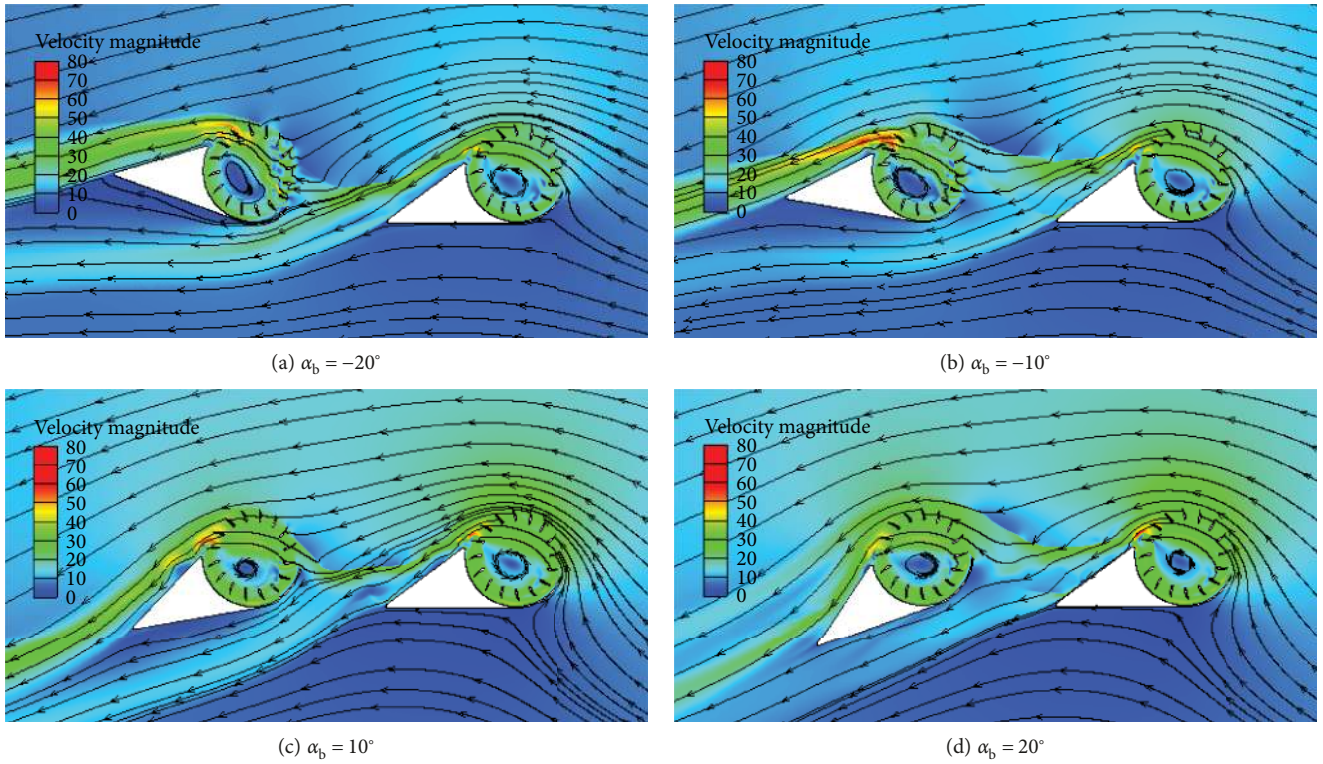

(a) $\alpha_b = -20^\circ$ (b) $\alpha_b = -10^\circ$

(c) $\alpha_b = 10^\circ$ (d) $\alpha_b = 20^\circ$

Figure 13: Velocity contours and streamlines of the lift and thrust of the front and rear fan wings when the front wing is fixed.

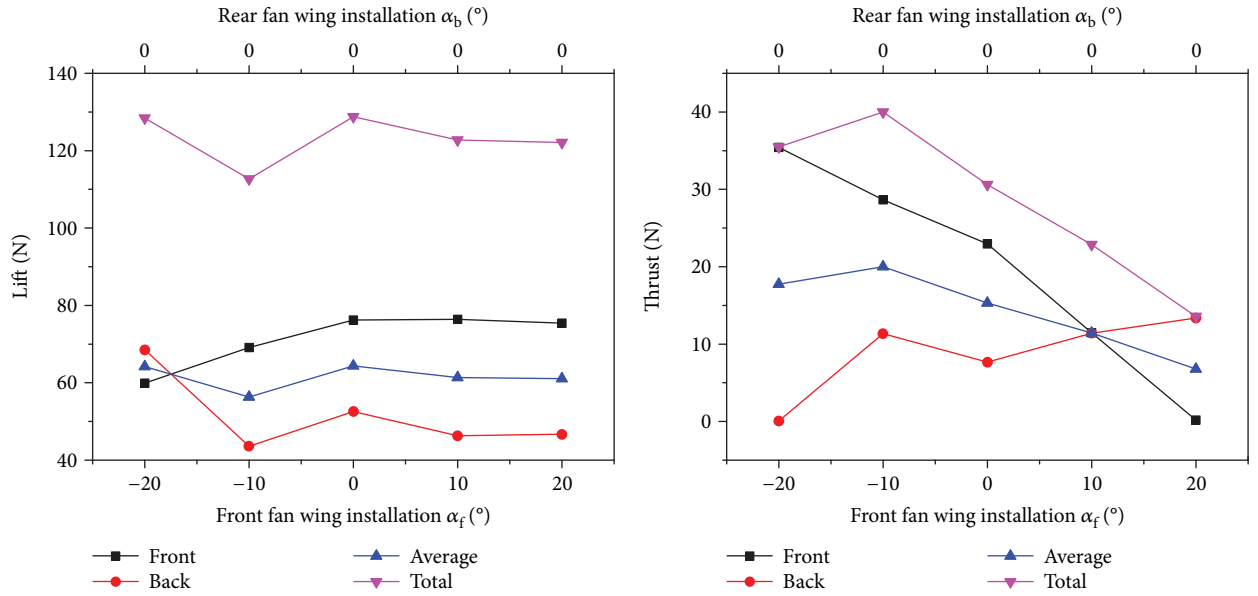

(a) Lift (b) Thrust

Figure 14: Curve of the lift and thrust of the front and rear fan wings when the rear wing is fixed.

in improving the overall aerodynamic force increase. As we can see from Figure 14(b), the average value of the thrust decreases with the increase of the front wing's installation angle. From the current flowchart, we can find that the streamline of the front wing's airflow is disturbed by the rear wing's airflow, and the airflow flowing into the rear wing decreases. Therefore, the rear wing's thrust continues to decrease. The rear angle $< 0^\circ$ value results in rather "odd" changes in lift and thrust behavior. This is due to the high energy fluid leaving the front fan wing entering the rear fan wing.

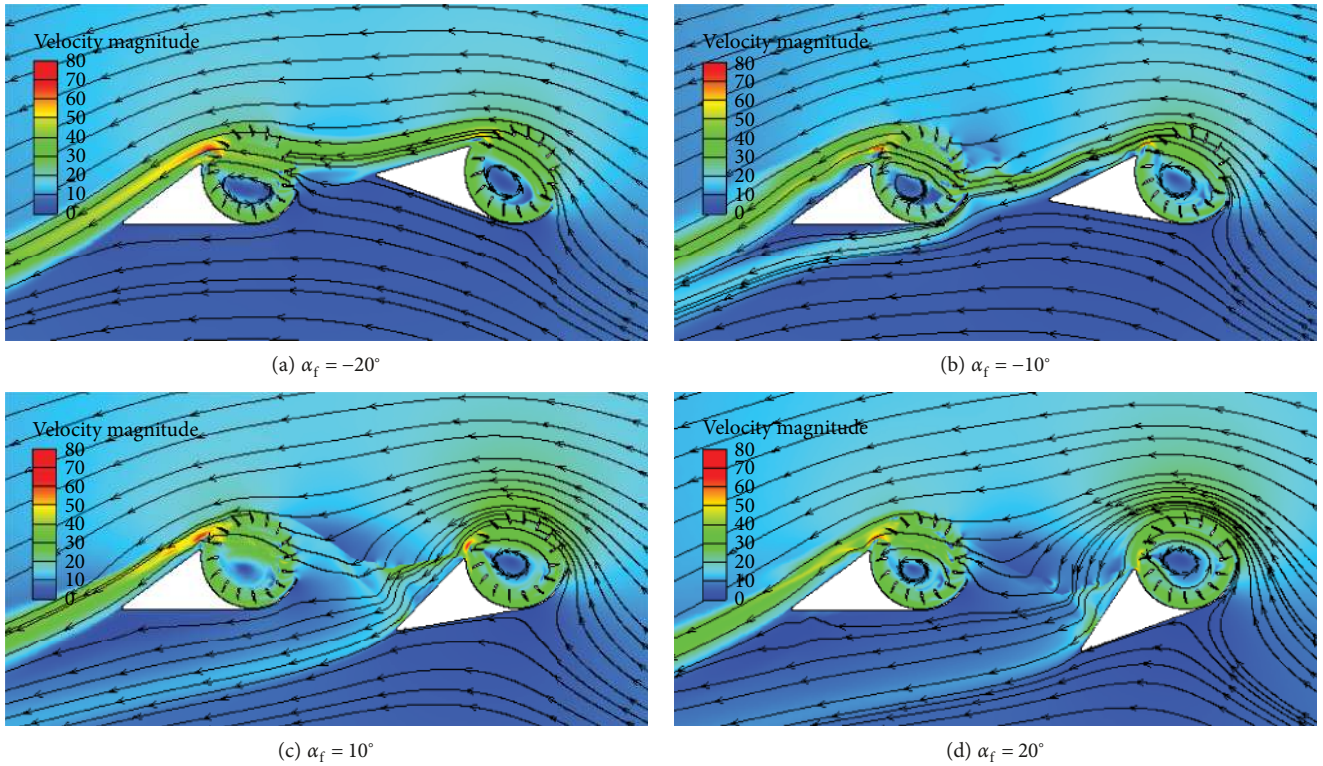

(a) $\alpha_f = -20^\circ$ (b) $\alpha_f = -10^\circ$

(c) $\alpha_f = 10^\circ$ (d) $\alpha_f = 20^\circ$

Figure 15: Velocity contours and streamlines of the lift and thrust of the front and rear fan wings when the rear wing is fixed.

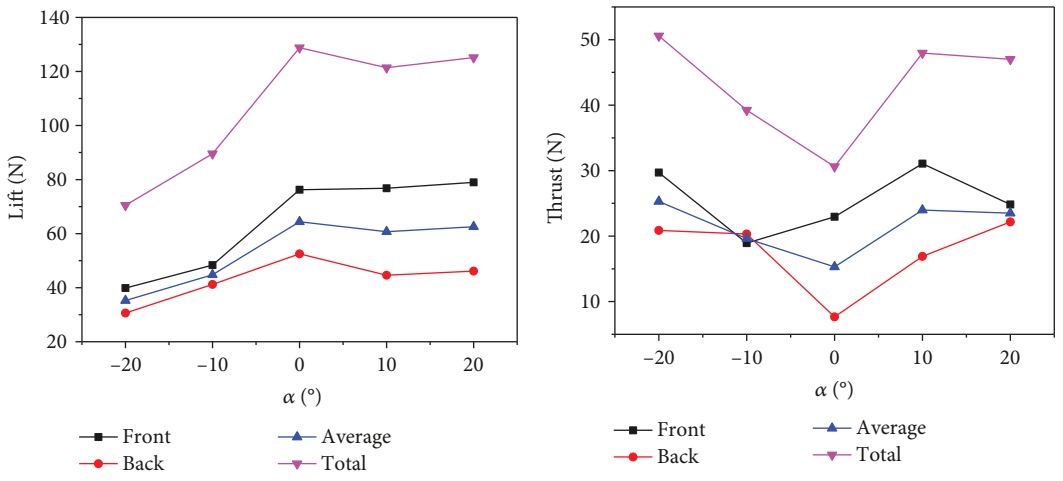

(a) Lift (b) Thrust

Figure 16: Curve of the lift and thrust of the front and rear fan wings when the front and rear wings have the same installation angle.

3.3.3. The Installation Angles of the Front and the Rear Fan Wings Are the Same. Under this situation, the installation angle of the front and the rear wings changes in the same way at the same time. As we can see from Figure 16(a), when the installation angles of the front and the rear wings are negative, the aerodynamic force increase effect keeps pace with the increase of the installation angles. When the installation angles of the front and the rear wings are positive, such an effect is not obvious. As is shown in Figure 16(b), the average thrust of both the front and rear wings hardly changes, which illustrates that the change of the installation angles of the front and the rear wings has little influence on the thrust. With analysis of Figure 17, flow separation does not occur when the installation angle of the front and the rear wings is large, which illustrates that the tandem fan wing possesses such aerodynamic characteristic, to keep the velocity streamline stable with the large installation angle. The phenomenon caused by the flow field is similar to the upper section.

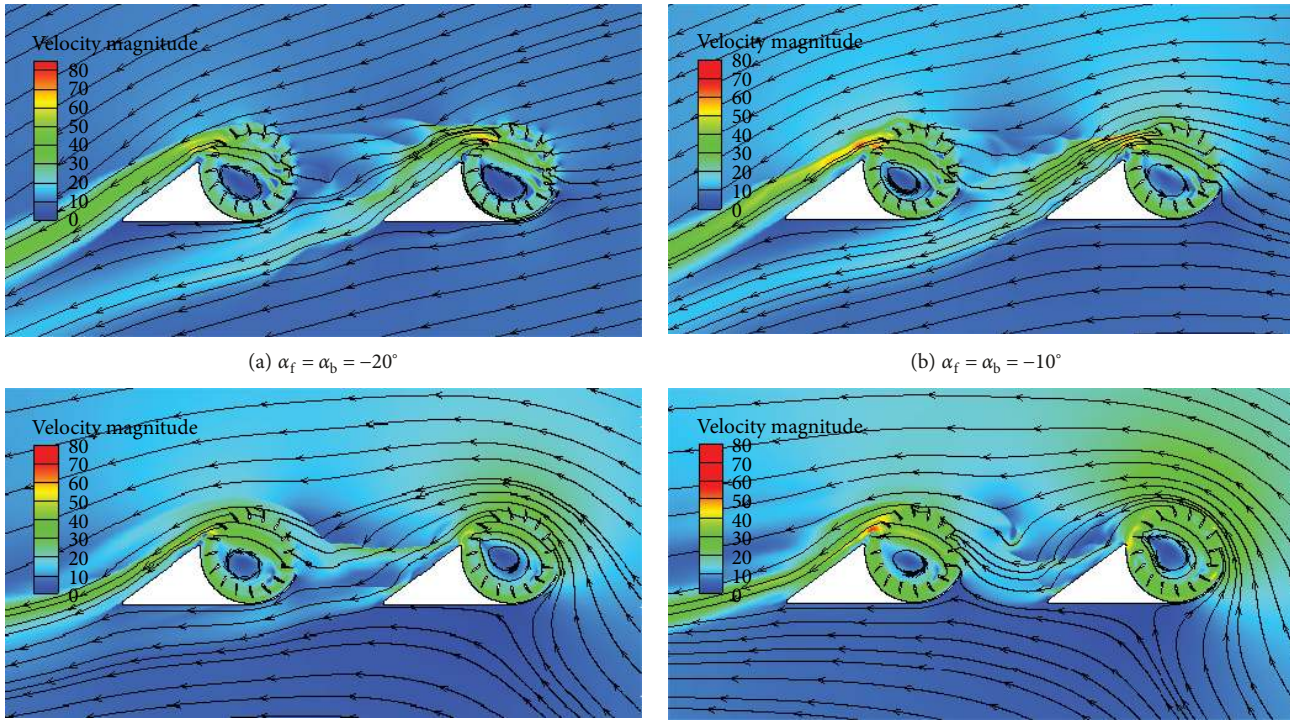

(a) $\alpha_f = \alpha_b = -20^\circ$ (b) $\alpha_f = \alpha_b = -10^\circ$

(c) $\alpha_f = \alpha_b = 10^\circ$ (d) $\alpha_f = \alpha_b = 20^\circ$

Figure 17: Velocity contours and streamlines of the front and rear fan wings when the front and rear wings have the same installation angle.

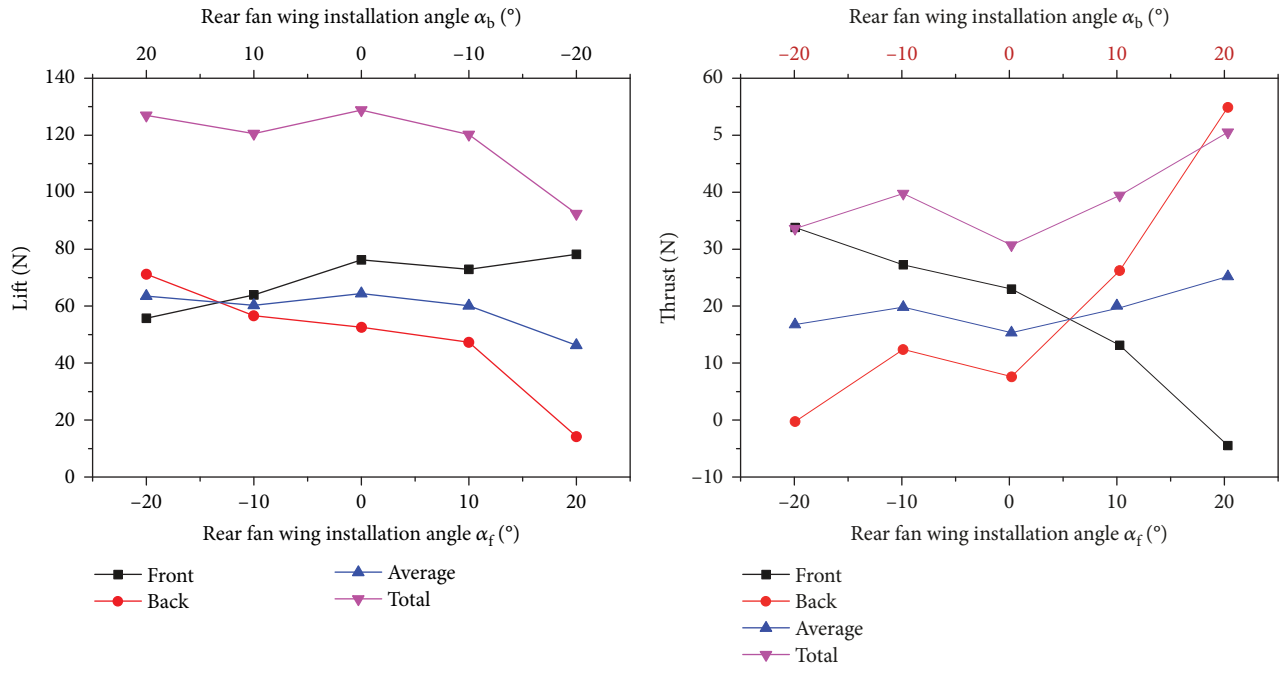

(a) Lift (b) Thrust

Figure 18: Curve of the lift and thrust of the front and rear fan wings when the front and rear wings have the opposite installation angle.

3.3.4. The Installation Angles of the Front and the Rear Fan Wings Are Different. The front and the rear wings change in a different direction at the same time with the front wing as the benchmark. Figure 18(a) shows that the lift of the rear wing is smaller than that of the front wing when the installation angle of the rear wing ranges from −20° to −10°. As we can see from the average value of the front and the rear wings' lift, the change of the average lift gradually decreases. As is

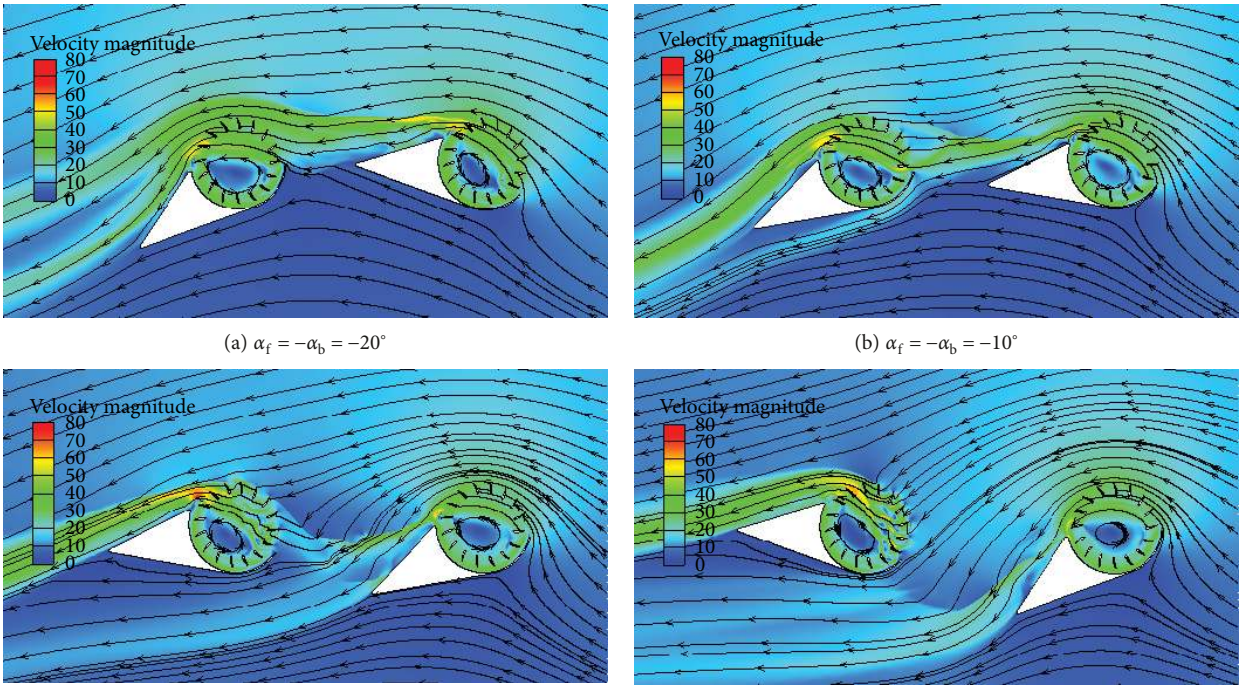

(a) $\alpha_f = -\alpha_b = -20^\circ$ (b) $\alpha_f = -\alpha_b = -10^\circ$

(c) $\alpha_f = -\alpha_b = 10^\circ$ (d) $\alpha_f = -\alpha_b = 20^\circ$

Figure 19: Velocity contours and streamlines of the front and rear fan wings when the front and rear wings have the opposite installation angle.

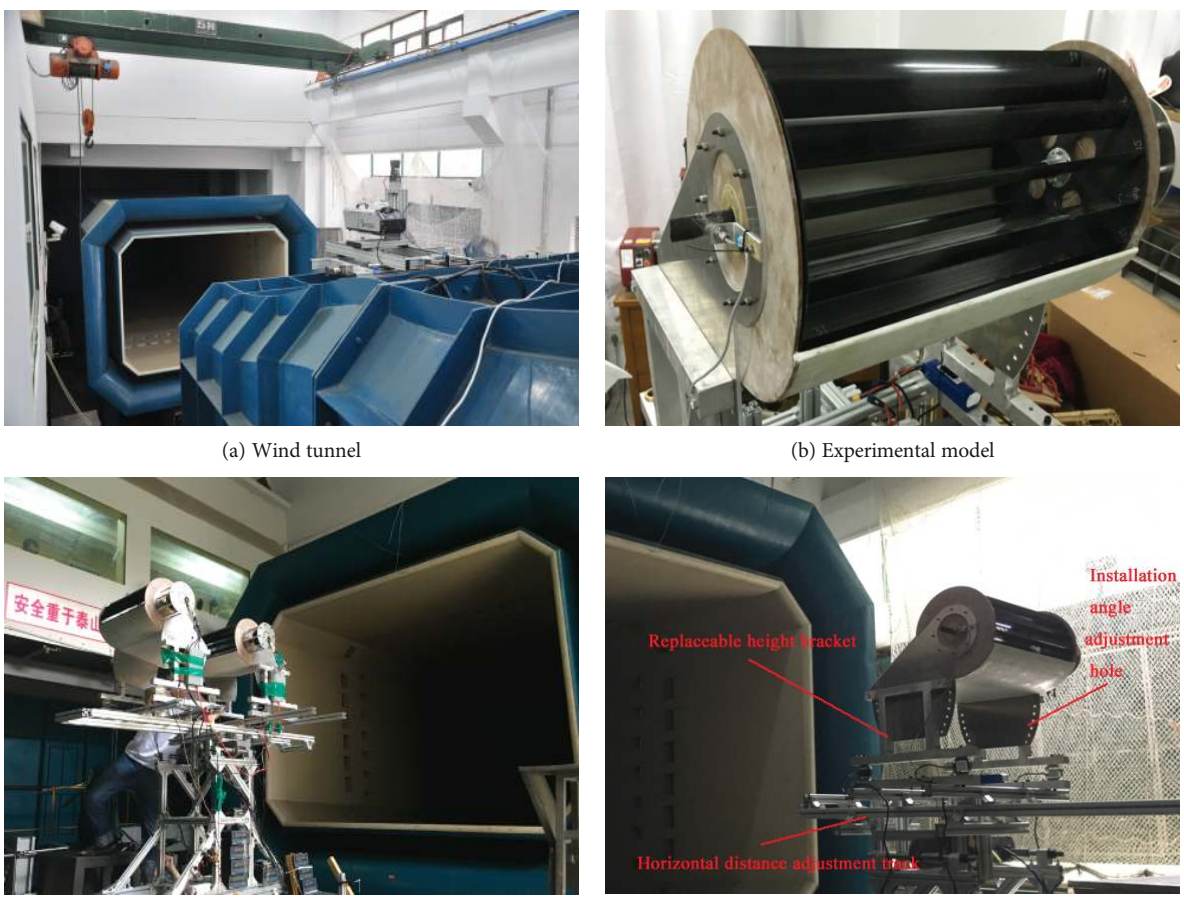

(a) Wind tunnel (b) Experimental model

(c) The position of the experimental model in the wind tunnel (d) The way of changing distance, height, and installation angle

Figure 20: Experimental model and equipment.

Table 3: Parameters of the wind tunnel.

Parameters	Value
Size of test area (m × m)	3.4 × 2.4
Maximum wind speed (m/s)	40
Minimum stable wind speed (m/s)	5
Shrinkage ratio	4

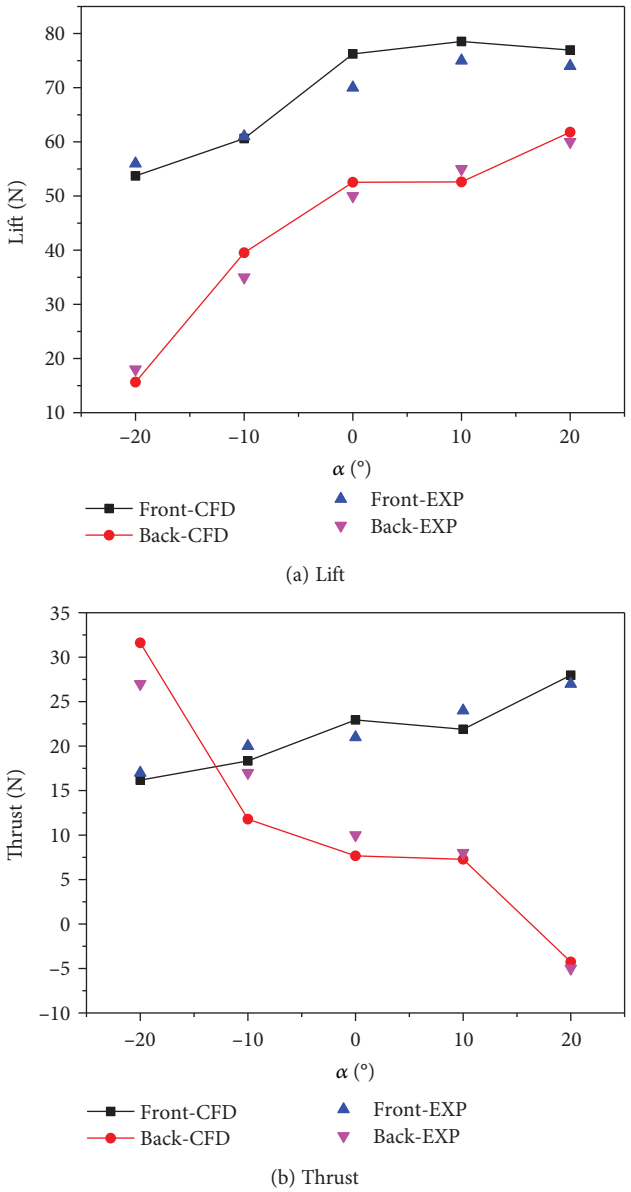

Figure 21: Comparison curves between numerical results and experimental results when the front wing is fixed.

shown in Figure 18(b), the thrust change still demonstrates the trend of substitution between the front and the rear wings. What is more, the average lift does not change too much. As we can see from Figure 19, when the installation angles of the front and the rear wings are the same and negative, the rear wing can get accelerated airflow from the front

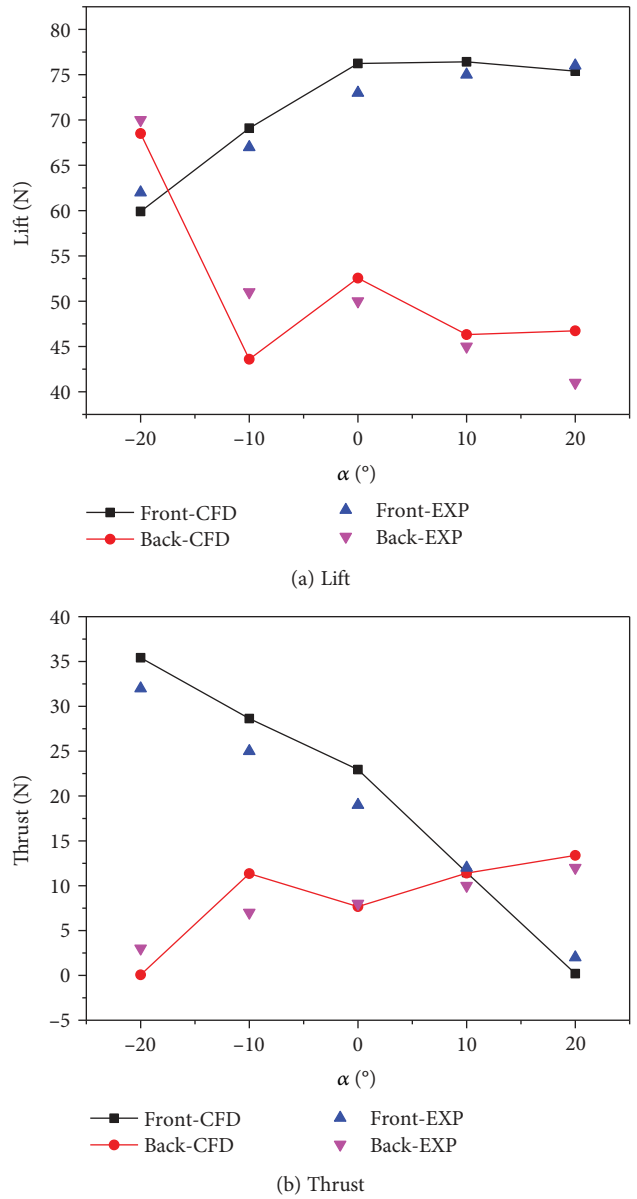

Figure 22: Comparison curves between numerical results and experimental results when the rear wing is fixed.

wing; at this time, the change of the front and the rear wings' lift and thrust is not obvious. When they are the same and positive, the rear wing cannot make use of the accelerated airflow from the front wing, which is indicated in the graph as the lift and thrust fluctuate greatly with the change of installation angle. The interference between the front and rear flow fields causes the abrupt flow field of the trailing edge of the front wing and the streamline bending.

4. Test Verification

4.1. Wind Tunnel and Model Arrangements. This experiment is based on the low-speed open return flow wind tunnel (Figure 20(a)), which is in the National Key Laboratory of Rotorcraft Aeromechanics in Nanjing University

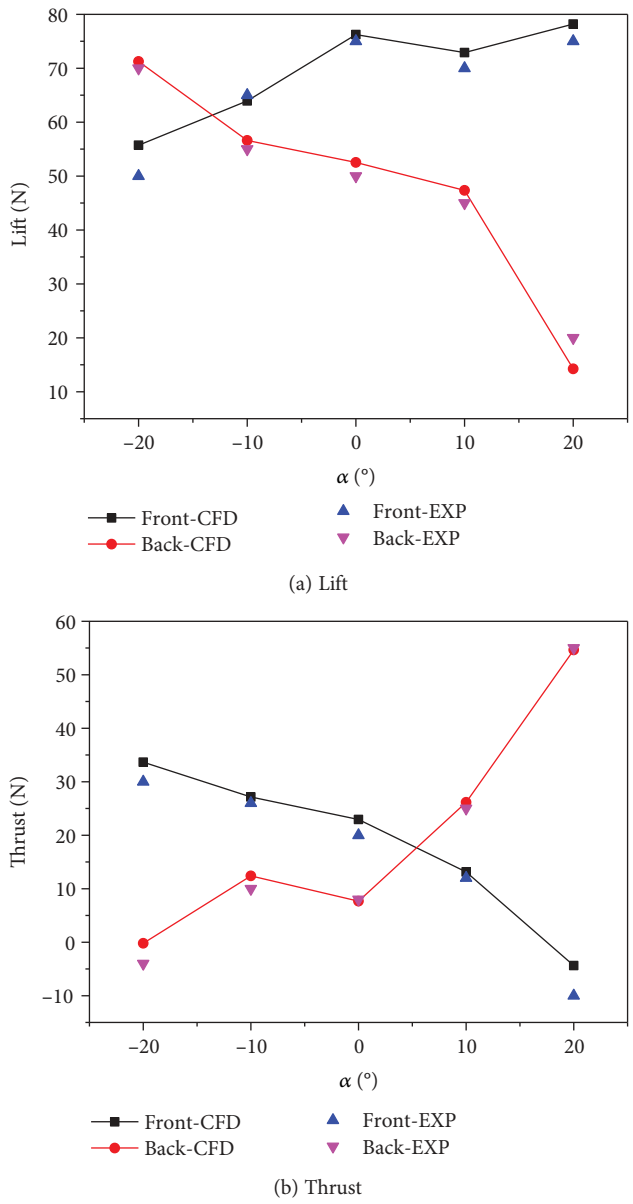

FIGURE 23: Comparison curves between numerical results and experimental results when the front and rear wings have the same installation angle.

of Aeronautics and Astronautics. The basic parameters of the experimental wind tunnel are shown in Table 3. The fan wing model (Figure 20(b)) used in this experiment is the same size as the numerical calculation model. The model airfoil is made of glass fiber, and the crossflow fan is made of carbon fiber material. The experimental bench is mainly composed of assembled aluminum. The whole experimental bench is placed in the relative position of the wind tunnel as shown in Figure 20(c). The way to change the distance between the front and rear wings is to move the front and rear wings along the horizontal guide rail. Pairs of bolts through the positioning holes on the wing plate change the installation angle of the wing. The height of the wing is changed by replacing different height brackets. Figure 20(d) shows the location of the adjusting element.

4.2. Experimental Results and Comparison. The comparison curves of the test results and numerical calculation results on the lift and the thrust of the front and the rear wings with different installation angles and under three conditions, namely, when the installation angle of the front wing is unchanged, when the installation angle of the rear wing is unchanged, and when the installation angles of the front and the rear wings are kept the same, are shown, respectively, in Figures 21–23. Although there exists some difference, the whole trend of change is the same. The relative error between most of the numerical calculation results and test results is less than 10%, which illustrates that the numerical calculation method is feasible in this paper, and it can be applied in more analyses of aerodynamic characteristics of the tandem fan wing.

5. Conclusion

A tandem fan wing configuration is studied by the CFD method. The numerical setup is validated by experiments performed on the model with a single wing. The aerodynamic performance of this configuration is studied for different relative positions of the wings. It is shown that the lift of the model increases up to a certain distance between the two wings in the free stream direction and then remains steady, but its thrust improves only when this distance is kept low. Also, the impact of the distance between the wings normal to the free stream direction on the aerodynamic performance of the configuration is studied, and it is shown that the best performance results when this distance is about zero. Moreover, the performance of the configuration is studied for different installation angles. It is shown that changing the installation angle does not improve the lift but it has some minor effects on the thrust.

Data Availability

The data used to support the findings of this study are available from the corresponding author upon request.

Conflicts of Interest

The authors declare that there is no conflict of interest regarding the publication of this paper.

Acknowledgments

The authors would like to acknowledge the financial support of the Priority Academic Program Development of Jiangsu Higher Education Institutions and useful information obtained from the FanWing company. The received funding did not lead to any conflict of interests.

References

[1] L. Meng, Y. Ye, and N. Li, "Research progress and application prospects of fan-wing aircraft," *Acta Aeronautica et Astronautica Sinica*, vol. 36, no. 8, pp. 2651–2661, 2015.

[2] G. R. Seyfang, "Fanwing-developments and applications," in *28th Congress of International Council of the Aeronautical Sciences, ICAS*, pp. 1–9, Brisbane, Australia, 2012.

[3] G. R. Seyfang, "Recent developments of the FanWing aircraft," in *The International Conference of the European Aerospace Societies, CEAS*, pp. 1–7, Venice, Italy, 2011.

[4] O. Ahad and J. M. R. Graham, "Flight simulation and testing of the fanwing experimental aircraft," *Aircraft Engineering and Aerospace Technology*, vol. 79, no. 2, pp. 131–136, 2007.

[5] N. Laing, "Fluid flow machine with parallel rotors," 1962, US Patent 3150821A.

[6] J. P. Hancock, "Test of a high efficiency transverse fan," in *16th Joint Propulsion Conference*, Hartford, CT, USA, 1980.

[7] G. J. Harloff, *Cross-Flow Fan Experimental Development and Finite-Element Modeling, Ph. D. Dissertation*, University of Texas at Arlington, Arlington, TX, USA, 1979.

[8] J. D. Kummer and T. Q. Dang, "High-lift propulsive airfoil with integrated crossflow fan," *Journal of Aircraft*, vol. 43, no. 4, pp. 1059–1068, 2006.

[9] T. Q. Dang and P. R. Bushnell, "Aerodynamics of cross-flow fans and their application to aircraft propulsion and flow control," *Progress in Aerospace Sciences*, vol. 45, no. 1-3, pp. 1–29, 2009.

[10] S. Askari and M. H. Shojaeefard, "Numerical simulation of flow over an airfoil with a cross flow fan as a lift generating member in a new aircraft model," *Aircraft Engineering and Aerospace Technology*, vol. 81, no. 1, pp. 59–64, 2009.

[11] S. Askari, M. H. Shojaeefard, and K. Goudarzi, "Experimental study of stall in an airfoil with forced airflow provided by an integrated cross-flow fan," *Journal of Aerospace Engineering*, vol. 225, no. 1, pp. 97–104, 2010.

[12] S. Askari and M. H. Shojaeefard, "Experimental and numerical study of an airfoil in combination with a cross flow fan," *Journal of Aerospace Engineering*, vol. 227, no. 7, pp. 1173–1187, 2012.

[13] S. Askari and M. H. Shojaeefard, "Shape optimization of the airfoil comprising a cross flow fan," *Aircraft Engineering and Aerospace Technology*, vol. 81, no. 5, pp. 407–415, 2009.

[14] N. Thouault, C. Breitsamter, and N. A. Adams, "Numerical and experimental analysis of a generic fan-in-wing configuration," *Journal of Aircraft*, vol. 46, no. 2, pp. 656–666, 2009.

[15] Z. F. Tang, M. Tang, and H. D. Wu, "The analysis of the influence of rotor anti-torque system's structure parameters on its aerodynamic influence," in *Proceeding of the 2nd Asian/Australian Rotorcraft Forum and the 4th International Basic Research Conference on Rotorcraft Technology*, pp. 1–9, Tianjin, China, 2013.

[16] Y. Lian, T. Broering, K. Hord, and R. Prater, "The characterization of tandem and corrugated wings," *Progress in Aerospace Sciences*, vol. 65, pp. 41–69, 2014.

[17] Z. Tong and M. Sun, "Flow analysis of twin-rotor configurations by Navier-Stokes simulation," *Journal of the American Helicopter Society*, vol. 45, no. 2, pp. 97–105, 2000.

[18] D. Siliang, T. Zhengfei, X. Pei, and J. Mengjiang, "Study on helicopter antitorque device based on cross-flow fan technology," *International Journal of Aerospace Engineering*, vol. 2016, Article ID 5396876, 12 pages, 2016.

[19] R. P. Tang, *Aerodynamic Experimental Research on Fan-Wing, M.S. Thesis*, Aeronautics and Astronautics Dept., Nanjing University of Aeronautics and Astronautics, 2014.